Photonirvachak
Journal of the Indian Society of Remote Sensing, Vol. 33, No. 4, 2005

STUDIES ON URBAN HEAT ISLANDS USING ENVISAT AATSR DATA

K.V.S. BADARINATH@, T.R. KIRAN CHAND, K. MADHAVI LATHA AND V. RAGHAVASWAMY*
Forestry & Ecology Division, National Remote Sensing Agency, Balanagar, Hyderabad – 500 037, India
*Land use and Urban Studies Group, National Remote Sensing Agency,
Balanagar, Hyderabad – 500 037, India
@Corresponding author : badrinath_kvs@nrsa,gov.in

ABSTRACT

Urbanization has significant effects on local weather and climate and among these effects one of the most familiar is the urban heat island, for which the temperatures of the central urban locations are several degrees higher than those of nearby rural areas of similar elevation. Satellite data provides important inputs for estimating regional surface albedo and evapotranspiration required in the studies related to surface energy balance. Present study describes the analysis of day and night ENVISAT-AATSR satellite data for Urban heat island and surface thermal inertia. Field campaigns have been conducted in synchronous with the satellite data over pass for validating the surface temperature estimated from AATSR data. Satellite derived surface temperature values are within $\pm 1^0$ C from ground measured values. Heat island formations in urban regions of Hyderabad and environs can be clearly seen in the night time data with core urban regions showing high temperatures. Apparent thermal inertia derived from AATSR day and night data sets have shown typical variations over urban regions.

Introduction

Urban Heat Islands (UHI) develop over cities as a result of anthropogenic activity, diverse surface cover and it represents the quality of climate over city. Studies on UHI help to understand the air quality, energy use, water use efficiency and human comfort. In cities, buildings and paved surfaces replace the existing green cover. Albedo is a measure of the amount of solar energy reflected by the surface. Surface temperature is prime importance to the study of urban climatology as it modulates the

Received 26 September, 2004; in final form 30 August, 2005

air temperature of the lowest layers of the urban atmosphere. Surface and atmospheric modifications due to urbanization generally lead to a modified thermal climate that is warmer than the surrounding non-urbanized areas, particularly at night. This phenomenon is known as "Urban Heat Island". The cause for occurrence of urban heat islands is due to removal of vegetation cover and paving of the land surface by non-evaporating and non-porous materials such as asphalt and concrete (Lo and Quattrochi, 2003). Urban heat island effect has been the subject of numerous studies in recent decades and is exhibited by many major cities around the world. These include Athens (Katsoulis *et al.*, 1985), Singapore and Kuala Lampur (Tso, 1996) and Washington, DC (Kim, 1992). Regional studies have also been carried out in Australia and Argentina (Camilloni and Barros, 1997), China (Wang *et al.*, 1990), South Korea (Lee, 1993) and the USA (Johnson *et al.*, 1994; Camilloni and Barros, 1997). There are a variety of reasons for the urban/rural temperature variance. The most significant of these are differences in the thermal properties of the radiating surfaces and a decreased rate of evapotranspiration in the urban environment. Oke (1982) lists several other factors in addition to these two. Contributions due to urban topography include the 'canyon effect' which increases absorption of shortwave radiation, a decreased sky view that reduces outgoing longwave radiation, and increased surface roughness, which reduces boundary layer winds and hinders sensible heat loss. High levels of pollution can increase the urban albedo and reradiate longwave radiation. Urban areas also exhibit a greater amount of anthropogenic heat generation. The present study addresses surface temperature estimation using AATSR data over urban regions for analyzing heat island formations. Advanced Along Track Scanning Radiometer (AATSR) is an advanced version of the ATSR system on board ERS-1 and 2. AATSR is a passive imaging instrument at 1 km resolution able to collect reflected and emitted electromagnetic radiation in 7 different spectral regions, spanning from the visible to the thermal infrared. The AATSR conical scanning mechanism allows the same area to be imaged twice at different viewing angles (nadir and 47 degrees forward) thus giving the possibility to estimate and correct for atmospheric effects and to improve the retrieval of Earth surface parameters.

Data Sets and Methodology

AATSR operates in channels with band centers at 0.555, 0.659, 0.858, 1.61, 3.70, 10.85 and 12 μm. NDVI estimated from AATSR has been taken as a parameter for estimating surface emissivity and algorithm based on nadir and forward scans of brightness temperature in 12 μm has been used for estimating surface temperature. ENVISAT AATSR data of March 6 and 7, 2003 has been used in the present study. The AATSR ATS_TOA_1C Level data has been obtained from European Space Agency (ESA) under Announcement of Opportunity (AO) Project. The present study explores the conceptual and methodological issues of taking NDVI of pure vegetation and bare pixels obtained form the reflectance's in near infrared (NIR) and Red channels and using the information for the calculation of vegetation cover. The percentage cover has been used for estimating emissivity at pixel level.

NDVI is defined as

$$NDVI = (\rho_2 - \rho_1)/(\rho_2 + \rho_1) \quad (1)$$

where, ρ_1, ρ_2 are the reflectance measured in red and NIR wavelength bands respectively.

Considering a mixed pixel with a proportion of vegetation over P_v and a soil proportion $(1-P_v)$, the NDVI value (i) as a first approximation is

$$i = i_v P_v + i_g (1 - P_v) \quad (2)$$

where i_v and i_g are the vegetation and ground NDVI values, respectively.

The vegetation fraction can be obtained from the NDVI by inverting equation (2). But this relationship is not correct (Price, 1990) because NDVI is a ratio and does not satisfy the associative property. This means that it is not the same, to weigh the reflectances in each channel and then calculate the NDVI, as the inverse procedure (applied to obtain equation 2).

A mixed pixel reflectance is

$$\rho_n = \rho_{nv} P_{v+} \rho_{ng} (1 - P_v) \quad (3)$$

where n = 1 for red and n=2 for near IR.

Substituting equation (3) into equation (1), the NDVI becomes

$$i = \frac{P_v(\rho_{2v} - \rho_{1v}) + (1 - P_v)(\rho_{2g} - \rho_{1g})}{P_v(\rho_{2v} + \rho_{1v}) + (1 - P_v)(\rho_{2g} + \rho_{1g})} \quad (4)$$

where ρ_{2v}, ρ_{1v} are reflectances in NIR and red region for pure vegetation pixels. ρ_{2g}, ρ_{1g} are reflectances in NIR and red region for pure soil pixels (Kant and Badarinath, 2000).

Equations (2) and (4) are not equivalent (Price, 1990). Depending on the reflectance values of each surface, the correction to equation (2) will be different. Thus, a better way to relate the NDVI to the vegetation cover is,

$$i = i_v P_v + i_g (1 - P_v) + di \quad (5)$$

where di is correcting factor obtained by subtracting equation (2) from equation (4).

The proportion of vegetation cover is calculated using the relation (Valor and Caselles, 1996),

$$P_v = (1 - i/i_g) / [(1 - i/i_g) - k(1 - i/i_v)] \quad (6)$$

where, $k = (\rho_{2v} - \rho_{1v}) / (\rho_{2g} - \rho_{1g})$

Finally, the relationship between emissivity (ε) and NDVI of a given surface is,

$$\varepsilon = a\, i + b \quad (7)$$

where, $a = (\varepsilon_v - \varepsilon_g)/(i_v - i_g)$ and $b = [\varepsilon_g(i_v + di) - \varepsilon_v (i_g + di)]/(i_v - i_g) + d\varepsilon$.

For a given area the coefficient 'a' is constant, while coefficient 'b', changes from pixel to pixel with the type of vegetation cover and surface structure. General behavior of the shape of curve corresponding to the relationship between emissivity and NDVI is quite similar to the combination of a straight line and a quadratic expression. In order to define the error in emissivity (dε) values per pixel, a quadratic form has to be used. The dε takes value zero for $P_v = 0$ and $P_v = 1$.

$$d\varepsilon = 4 < d\varepsilon > P_v (1 - P_v) \quad (8)$$

where <dε> is mean weighted value taking into account the different vegetation in the area, their structures and their proportions in it. The maximum value of dε is given by <dε> and with a separation between boxes varying with P_v.

The following algorithm has been used for deriving surface temperature using AATSR data.

$$T_s = T_n + A*(T_n - T_f) + (1 - e)*B_1 - De * B_2$$

where A, B_0, B_1, B_2 are the double-angle coefficients. Based on the measured values of water vapor using MICROTOPS-II ozonometer which are in the range 0.9 to 1.1g/cm^2, the values of coefficients have been taken as A = 1; B_1 = 40; B_2 = 40 (Sobrino *et al.*, 1996); T_n and T_f are nadir and forward brightness temperatures at 12 mm. Portable meteorological kit has been used for measuring wind speed, wind direction, relative humidity and air temperature. Soil temperature probe has been used to measure soil temperature at 5 cm depth. Telatemp Model AG-42 IR thermometer has been used for estimating crop and soil surface temperature in field in synchronous with ENVISAT satellite pass. The instrument operates in the wavelength range 8 - 14 mm with an accuracy of ± 0.5°C and resolution of ± 0.1°C.

Thermal inertia, *TI*, is a physical property of materials describing their impedance to temperature change. The equation $TI = (K\rho c)^{1/2}$, shows its dependence on the thermal conductivity K, density ρ and specific heat *c* of the material. The change in temperature at the Earth's surface due to a given heat flux is inversely related to the thermal inertia of the exposed material. In particular, water bodies, having *TI* higher than dry soils and rocks, exhibit lower diurnal temperature fluctuations. As soil water content increases, thermal inertia also increases, reducing the diurnal temperature range. Present satellite remote sensing capabilities in measuring Earth surface temperature can be exploited in order to derive information on soil moisture, provided that the re-visitation time is adequate to follow the diurnal temperature cycle and the spectral resolution is sufficient to evaluate the net heat flux at the Earth surface. An approximate value of the actual thermal inertia (*TI*) called Apparent Thermal Inertia (*ATI*), can be obtained from ENVISAT AATSR measurements of the spectral surface albedo *A* and of the diurnal temperature range *DT*, as $ATI = (1 - A)/DT$. Surface albedo *A* was obtained using visible and near-infrared reflectances from AATSR channels using the relation Albedo = $\sum\rho_i E_i / \sum E_i$ where 'ρ_i' is reflectance in AATSR channels centered at 0.555, 0.659, 0.858 μm and E_i is solar exoatmospheric irradiance in each channel . The diurnal temperature range *DT* is the difference between surface temperatures, *T*, measured in the AATSR thermal infrared channel at noon and midnight $DT = (T_{12\mu m}day - T_{12\mu m}\ night)$. Actual values of *TI* and measured *ATI* are variously affected by parameters related to space-time variability of observational, atmospheric, and surface conditions (e.g. time of the pass, satellite/solar zenith angles, transmittance, cloud cover, vegetation).

Results and Discussion

Fig. 1a shows the AATSR bands 0.87, 0.67 and 0.55 μm FCC of study area. Land use/land cover map of the study area is given in Fig.2. The determination of surface temperature from satellite data requires the knowledge of emissivity of various land surface features at the sensor resolution. In the present methodology, the determination of surface emissivity requires the use of satellite data together with some emissivity values of vegetation types from literature. Since, we do not have prior information on emissivity values of the area, the mean emissivity value of 0.88 for bare soil and 0.986 for vegetation in 8-14 μm region has been taken (Carnahan and Larson, 1990). The emissivity values over soil have been confirmed with the field measurements on measured soil temperature and radiant temperature. The mean value of $<d\varepsilon>$ has been taken as 0.01. Calculation of proportion of vegetation cover needs reflectance of pure pixels of vegetation and bare soils in NIR and Red channels and these values have been taken from the AATSR data gridded (AATSR product type ATS_TOA_1C) provided by ESA. The maximum NDVI value in the present data set is 0.65 and minimum of 0.11. The proportion of vegetation cover has been calculated using equation (6). Percentage vegetation cover (P_v) image generated from AATSR is shown in Fig. 1b and the values of P_v vary depending on the proportion of vegetation in the 1 km resolution pixel. Surface emissivity per pixel has been estimated using equation (7). Emissivity image generated from AATSR is shown in Fig. 1c. The emissivity values derived from the present methodology have been compared with values in 8-14 μm range over some known features and are provided in Table-1 (Valor and Caselles, 1996) and are found to be in reasonable agreement with an error not exceeding 1%. Surface temperature estimated using day and night time data of AATSR is shown in Fig. 1d and 1e). Field campaigns in synchronous with satellite overpass have been conducted and the comparison of field measured surface temperature with satellite data over crop and fallow areas suggested possible of ~± 1°K. The values of surface temperature estimated using AATSR has been found to be in acceptable range over the study area. The surface temperature is low over water surface (18-21°C) and maximum over urban areas (36-40°C). Apparent thermal inertia image generated from day and night surface temperature data of AATSR has been shown in Fig. 1f. Apparent thermal inertia derived from AATSR showed typical variations matching with urban land use variations viz., dense,

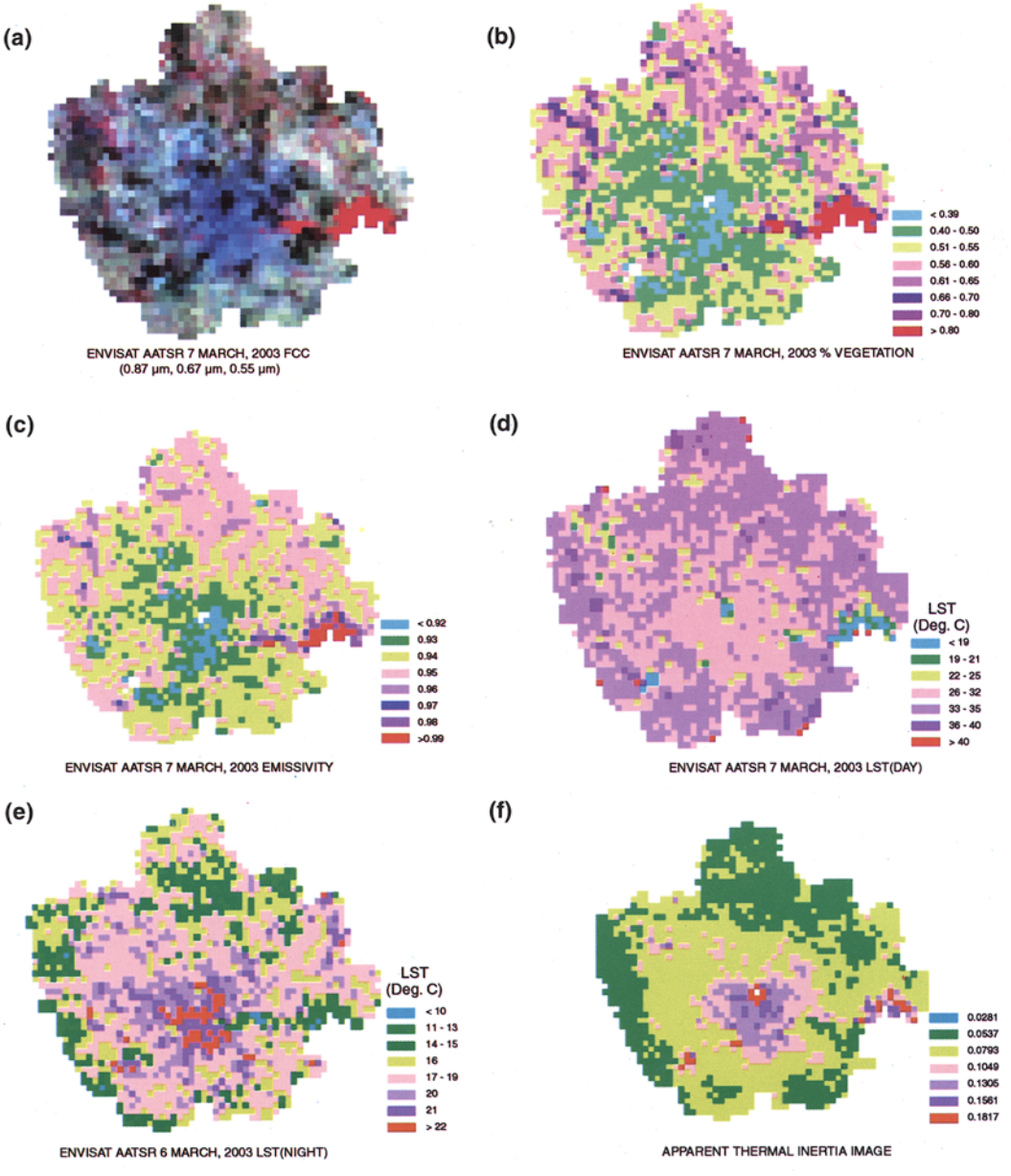

Fig. 1. (a) False Color Composite (FCC) of visible and near-IR bands of AATSR
(b) Percentage vegetation map generated from NDVI derived from AATSR
(c) Emissivity image generated from % vegetation cover information
(d) Land surface temperature image derived from AATSR data during daytime
(e) AATSR derived Land surface temperature image during night time
(f) Apparent Thermal Inertia (ATI) image generated from AATSR day and night time temperature variation and albedo.

medium and sparse urban areas (Fig. 2). The scatter plot between albedo and surface temperature estimated from AATSR data is shown in Fig. 3. It can be seen from Fig. 3 that surface temperature shows expected positive correlation with albedo for different features. The information on urban heat island formation and its spatial variation at 1 km resolution from AATSR provides planners a broad overview over temperature variation over urban areas. This information coupled with other data from high resolution sensors can be used to incorporate mitigation measures such as zone wise avenue plantations, recreational parks with vegetation cover etc.

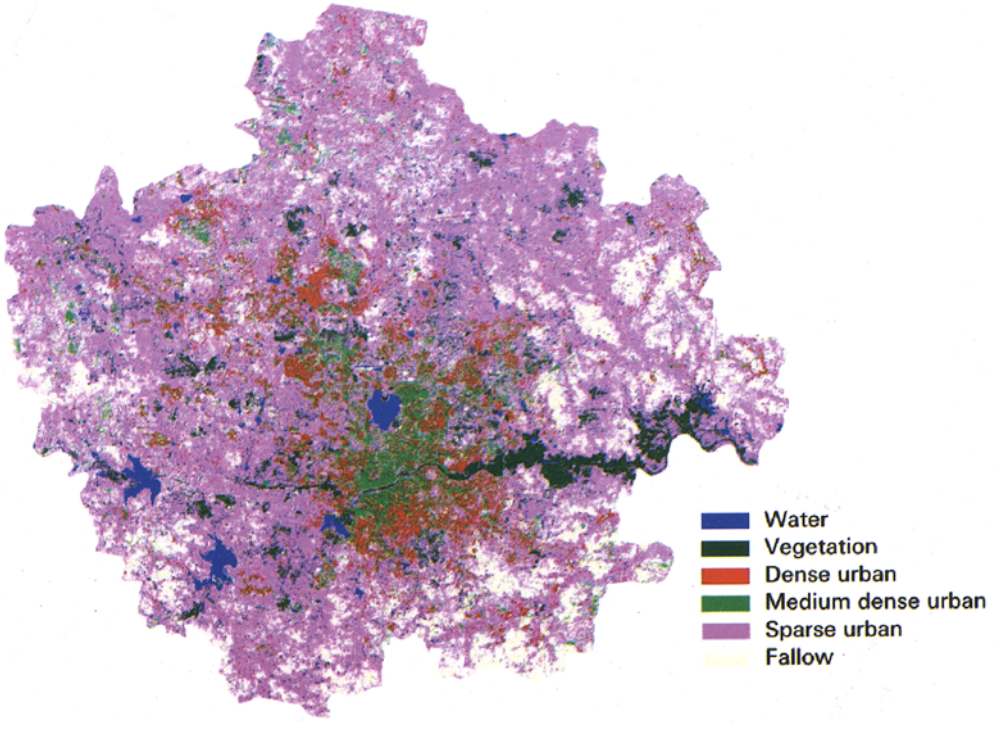

Fig. 2. Land use/land cover map of the study area

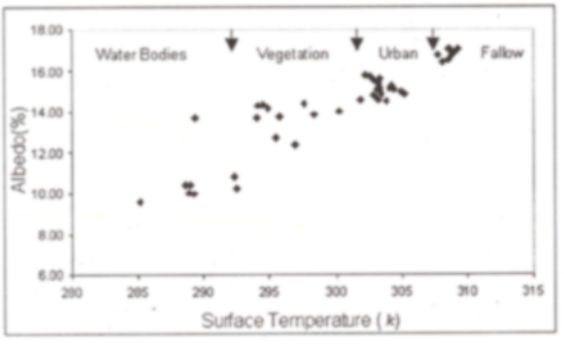

Fig. 3. Scatter plot showing relation between albedo and surface temperature estimated from AATSR data

Table 1: Emissivity values of different features estimated using AATSR data based on percentage vegetation cover

Land Use / Land cover feature	Emissivity Value
Dense urban	0.938±0.007
Medium dense urban	0.955±0.006
Sparse urban	0.968±0.003
Water	0.997±0.003
Vegetation	0.985±0.002

Conclusion

Day and night time data sets of ENVISAT AATSR data over urban areas of Hyderabad have been analyzed with a view to study the urban heat island formation. The analysis of data shows that:

- Temperature variations during day and nighttime correlated well with the density patterns of urban areas.
- Spatial variation in apparent thermal inertia estimated from the AATSR data showed positive correlation with variability in land use/ land cover in urban areas.
- The information on urban heat island formations in city areas can be used for urban planning activities in terms of avenue plantations and recreational parks for reducing the heat island formation.

Acknowledgements

Authors are grateful to Director, NRSA and Deputy Director (RS&GIS-AA), NRSA for their help and encouragement and ISRO-GBP for funding support. The authors are thankful to ESA for providing AATSR data as a part of Announcement of Opportunity Project ID 887.

References

Camilloni, I. and Barros, V. (1997). On the urban heat island eVect dependence on temperature trends. *Climatic Change*, **37**: 665-681.

Carnahan, W.H. and Larson, R.C. (1990). An analysis of an urban heat sink. *Remote Sensing of Env.*, **33**: 65-71.

Johnson, G.L, Davis, J.M., Karl, T.R., McNab, A.L., Gallo, K.P., Tarpley, J.D. and Bloomfield, P. (1994). Estimating urban temperature bias using polar-orbiting satellite data. *Journal of Applied Meteorology*, **33**: 358-369.

Kant, Y. and Badarinath, K.V.S. (2000). Studies on Land Surface Temperature over heterogeneous areas using AVHRR data. *Int. J. Remote Sensing*, **21(8)**: 1749-1756.

Kim, H.H. (1992). Urban heat island. *Int. J. of Remote Sensing*, **13**: 2319-2336.

Katsoulis, B.D. and Theoharatos, G.A. (1985). Indications of the urban heat island in Athens, Greece. *Journal of Climate and Applied Meteorology*, **24**: 1296-1302.

Lee, H. (1993). An application of NOAA AVHRR thermal data to the study of urban heat islands. *Atmospheric Environment*, **27B**: 1-13.

Lo, C.P. and Quattrochi, D.L. (2003). Land-use and Land-cover change, urban heat island phenomenon and health implications: A Remote Sensing Approach. *Photogrammetric Engineering and Remote Sensing*, **69(9)**: 1053-1063.

Oke, T.R. (1982). The energetic basis of the urban heat island. *Quarterly Journal of the Royal Meteorological Society*, **108**: 1-24.

Price, J.C. (1990). Using spatial context in satellite data to infer regional scale evapotranspiration. *IEEE Trans. Geoscience and Remote Sensing*, **28**: 940-948.

Sobrino, J.A., Li, Z.L., Stoll, P. and Becker, F. (1996). Multi-channel and multi-angle algorithms for estimating sea and land surface temperature with ATSR data. *Int. J. of Remote Sensing*, **17**: 2089-2114.

Tso, C.P. (1996). A survey of urban heat island studies in two tropical cities. *Atmospheric Environment*, **30**: 507-519.

Valor, E. and Caselles, V. (1996). Mapping Land surface emissivity from NDVI : Application to European, African & South American Areas. *Remote Sensing of Env.*, **57**: 167-184.

Wang, W., Zheng, Z. and Karl, T.R. (1990). Urban heat islands in China. *Geophysical Research Letters*, **17**: 2377-2380.